View metadata, citation and similar papers at core.ac.uk
brought to you by CORE
provided by KITopen

Electroweak $t\bar{t}$ hadroproduction in the presence of heavy Z' and W' bosons at NLO QCD in POWHEG

Mohammad Mahdi Altakach,[1,2,*] Tomáš Ježo,[3,†] Michael Klasen,[2,‡] Jean-Nicolas Lang,[4,§] and Ingo Schienbein[1,‖]

[1]*Laboratoire de Physique Subatomique et de Cosmologie, Université Grenoble-Alpes, CNRS/IN2P3, 53 Avenue des Martyrs, 38026 Grenoble, France*

[2]*Institut für Theoretische Physik, Westfälische Wilhelms-Universität Münster, Wilhelm-Klemm-Straße 9, 48149 Münster, Germany*

[3]*Institut für Theoretische Physik, Karlsruhe Institut für Technologie, 76128 Karlsruhe, Germany*

[4]*Physik-Institut, Universität Zürich, 8057 Zürich, Switzerland*

(Received 18 January 2021; accepted 18 May 2021; published 22 June 2021)

We present a new calculation of next-to-leading order QCD corrections to electroweak top-quark pair hadroproduction in extensions of the Standard Model (SM) with extra heavy neutral and charged spin-1 resonances which considerably extends and improves an earlier calculation performed by some of us. In particular, we allow for flavor-non-diagonal Z' couplings and take into account nonresonant production in the SM and beyond including the contributions with t-channel W and W' bosons. As a result, models with a more complicated flavor structure which have been proposed to explain the flavor anomalies in B decays can now be accommodated in our code. Moreover, the new t-channel contributions lead to improved cross sections predictions at higher energies beyond the LHC reach. All amplitudes are generated using the RECOLA2 package. As in our previous work, we include next-to-leading order QCD corrections and consistently match to parton showers with the POWHEG method fully taking into account the interference effects between the SM and new physics amplitudes. We consider the sequential Standard Model, the topcolor model, as well as the third family hypercharge model featuring non-flavor-diagonal Z' couplings and present numerical results for $t\bar{t}$ cross sections at hadron colliders with a center-of-mass energy up to 100 TeV.

DOI: 10.1103/PhysRevD.103.115026

I. INTRODUCTION

The Standard Model (SM) of particle physics, based on an $\mathrm{SU}(3)_C \times \mathrm{SU}(2)_L \times \mathrm{U}(1)_Y$ gauge symmetry, is an extremely successful theory that accounts for a wide range of experimental measurements at both the intensity and energy frontiers. Nevertheless, it is widely believed to be incomplete for different reasons. On the observational side, the SM does not include gravity, it does not provide a candidate for a cold dark matter particle, the CP-violating phase of the SM CKM (Cabibbo-Kobayashi-Maskawa) matrix is not sufficient to explain the matter-antimatter asymmetry observed in the Universe, and massive neutrinos are, *a priori*, not accounted for in the SM. In addition, the SM and in particular its scalar sector suffer from a variety of naturalness problems raising the questions why CP violation in the strong interaction is absent or at least strongly suppressed and why the Higgs boson mass is stable under quantum corrections. On the aesthetical side, it is not clear why the SM gauge group is a direct product of three independent symmetry factors, why there are three generations of fermions, why their masses span several orders of magnitude, and what gives rise to the complicated pattern in the CKM and Pontecorvo-Maki-Nakagawa-Sakata mixing matrices. The general expectation has therefore been for a long time that close to the electroweak scale new physics beyond the SM should be present, which allows one to at least partially understand the structure of the SM and avoid fine-tuning its 26 free parameters.

Despite the fact that no signals of new physics have been found in the first two runs of the Large Hadron Collider (LHC) at CERN, there are still high hopes that new particles will show up in the future high-luminosity runs of the LHC. It is also clear that such signals will likely appear as small deviations from the SM predictions, which makes precision calculations of both the SM background and the new physics signals increasingly important. The focus of this paper is on models with new heavy,

*altakach@lpsc.in2p3.fr
†tomas.jezo@kit.edu
‡michael.klasen@uni-muenster.de
§jlang@physik.uzh.ch
‖ingo.schienbein@lpsc.in2p3.fr

Published by the American Physical Society under the terms of the Creative Commons Attribution 4.0 International license. Further distribution of this work must maintain attribution to the author(s) and the published article's title, journal citation, and DOI. Funded by SCOAP³.

electrically charged or neutral spin-one resonances, usually denoted by W' and Z', respectively. Such resonances are predicted by several well-motivated extensions of the SM, e.g., grand unified theories, theories with a new strong interaction at the TeV scale, or models with large extra dimensions, and are extensively sought after by three of the experimental collaborations (ATLAS, CMS and LHCb) at the LHC. In this respect it is noteworthy that Z' models with a nonuniversal flavor structure [1–4], where the Z' couples differently to the fermions of the three SM families, are viable candidates to explain the current B-flavor anomalies [5–14].

In many cases, the strongest constraints on the parameter space of models with Z' and W' resonances come from searches with dilepton final states [15,16]. In this case, precise predictions at next-to-leading order (NLO) of QCD including the resummation of soft gluon terms at next-to-leading logarithmic accuracy can be obtained with the RESUMMINO code [17,18], which has been used previously to derive limits on Z' and W' masses using data for dilepton final states [19,20] and to provide predictions for the high-energy/high-luminosity options of the LHC [21]. However, top-quark observables are also very interesting since the third generation plays a prominent role in the SM due to the large Yukawa coupling of the top quark. Therefore, it is quite conceivable that new gauge bosons, similarly to the Higgs boson, couple predominantly to the top quark [22]. In 2015, some of us performed a calculation of next-to-leading order QCD corrections to the electroweak (EW) $t\bar{t}$ production in the presence of a Z' resonance [23]. The calculation properly accounted for the interference between SM and new physics amplitudes in a semiautomated fashion. It was implemented in the POWHEG BOX framework [24–26], that allows for a consistent matching of the fixed NLO calculation with Parton shower (PS) Monte Carlo generators. The NLO + PS results obtained with this tool, dubbed PBZP, are useful since they bridge the gap between first-principles higher-order calculations and the complex detector signatures and data of the experimental community. The PBZP code is therefore regularly used in Z' searches by the ATLAS and CMS collaborations [27–33].

In this article, we present a new calculation of NLO QCD corrections to electroweak top-quark pair hadroproduction in extensions of the Standard Model with extra heavy neutral and charged spin-1 resonances which considerably extends and improves an earlier calculation performed by some of us which was implemented in the code PBZP. (i) The amplitudes have been calculated using the RECOLA2 package [34]. This package has been designed to automate the calculations of amplitudes in theories beyond the SM including QCD and electroweak corrections at NLO. Our calculation is one of the first to use and validate this tool for a BSM (beyond the Standard Model) calculation. Implementing the amplitudes obtained with RECOLA2 into Monte Carlo event generators, here within the POWHEG BOX framework is an important aspect since it makes the tool more useful for the LHC experiments. (ii) The new code can now deal with a more general flavor structure of the couplings of the new heavy resonances to the Standard Model fermions which considerably increases the difficulty of the calculation due to its much larger complexity and the level of technical sophistication. As a result of this effort, Z' models which have been proposed in the literature to explain the B-flavor anomalies can now be implemented in our code. (iii) Another new feature is that the calculation now includes t-channel W and W' contributions. We study their importance numerically as a function of both the new gauge boson mass and the collider energy and propose useful kinematic cuts to disentangle the different contributions. As we will show, including the t-channel contributions leads to improved cross section predictions at higher energies beyond the LHC reach. (iv) As before, all interference terms are fully taken into account, and the photon induced channels for the SM are included, properly matched within POWHEG. As discussed in Ref. [23] the latter can give a sizable contribution to the cross section. This work paves the way for a similar calculation of the NLO QCD corrections to the process $pp \to W/W'/Z' \to t\bar{b}$ using RECOLA2 for the generation of the amplitudes and including a proper implementation within the POWHEG BOX framework.

The remainder of this paper is organized as follows: in Sec. II we define the production of top-quark pairs at hadron colliders including new electroweak gauge bosons, focusing on the perturbative organization of the cross section and its contributions at leading and next-to-leading order in the strong and electroweak coupling constants. In Sec. III we describe our calculation with a focus on the aspects that differ from our previous calculation in Ref. [23]. This discussion should be useful for other RECOLA2-based calculations in the future. Next, in Sec. IV we summarize the models for which we present numerical results in Sec. V. In addition to a study of the effect of cuts we will show results for fiducial cross sections for a range of heavy resonance masses and different center-of-mass energies. Here, the purpose is to present the new features of the PBZP code instead of aiming at exhaustive phenomenological studies of these models which we leave for future work. Finally, in Sec. VI we present a summary and our conclusions.

II. HADROPRODUCTION OF TOP-QUARK PAIRS

The cross section for the hadroproduction of a $t\bar{t}$ pair, $AB \to t\bar{t}X$, is given by a convolution of the parton distribution functions (PDFs) inside the two incoming hadrons $[f_{a/A}(x_a, \mu_F), f_{b/B}(x_b, \mu_F)]$ with the short distance cross sections $[d\hat{\sigma}_{ab}]$:

$$d\sigma = \sum_{ab} \int f_{a/A}(x_a, \mu_F) f_{b/B}(x_b, \mu_F) \times d\hat{\sigma}_{ab}(\mu_R, \mu_F) dx_a dx_b. \quad (1)$$

Here, μ_F and μ_R are the factorization and renormalization scales, respectively, and a sum over all relevant partonic channels, $ab \to t\bar{t}X$ is performed. This sum depends on various details like the heavy flavor scheme, the perturbative order and the model. Here we work in a 5-flavor number scheme (5-FNS) including all relevant contributions with u, d, s, c, b (anti)quarks, gluons and unless explicitly stated also photons in the initial state.

Up to next-to-leading order the hard scattering cross sections have the following perturbative expansion in the strong (α_s) and electroweak (α) coupling constants:

$$\hat{\sigma} = \hat{\sigma}_{2;0}(\alpha_S^2) + \hat{\sigma}_{3;0}(\alpha_S^3) + \hat{\sigma}_{2;1}(\alpha_S^2\alpha) + \hat{\boldsymbol{\sigma}}_{\mathbf{0;2}}(\boldsymbol{\alpha^2}) + \hat{\boldsymbol{\sigma}}_{\mathbf{1;2}}(\boldsymbol{\alpha_S\alpha^2}) + \hat{\boldsymbol{\sigma}}_{\mathbf{1;1}}(\boldsymbol{\alpha_S\alpha}) + \hat{\sigma}_{0;3}(\alpha^3), \quad (2)$$

where the numerical indices $(i;j)$ in $\hat{\sigma}_{i;j}$ represent the powers in α_s and α, respectively, and the dependence on the renormalization and factorization scales and the parton flavor indices "ab" have been suppressed. We now briefly describe the different contributions where the terms highlighted in bold have been included in our calculation:

(i) $\hat{\sigma}_{0;2}$, $\hat{\sigma}_{1;2}$. In this paper, we focus on the tree-level electroweak top-quark pair production, $\hat{\sigma}_{0;2}$, and the NLO QCD corrections to it, $\hat{\sigma}_{1;2}$. $\hat{\sigma}_{0;2}$ receives contributions from the s-channel amplitudes $q\bar{q} \to (Z', Z, \gamma) \to t\bar{t}$ including the Z' signal and its interference with the photon and SM Z boson. Due to the resonance of the Z' boson, we expect these terms to be the most relevant for new physics searches. In addition, we include new contributions from diagrams with nonresonant t-channel exchange of W, W' and Z' bosons that were not considered in Ref. [23]. Note that, out of these, the first two take into account CKM mixing and the last one is only allowed in models with flavor-non-diagonal couplings due to the absence of a top quark PDF in a 5-FNS. A particular advantage of the $\hat{\sigma}_{0;2}$ contribution is that the calculation of higher order QCD corrections to it, $\hat{\sigma}_{1;2}$, can be carried out in a model-independent way.

(ii) $\hat{\sigma}_{1;1}$. We also consider the term $\hat{\sigma}_{1;1}$ which receives contributions from the photon induced subprocess $\gamma g \to t\bar{t}$ and the previously not considered interference of the s-channel QCD and the t-channel electroweak top-pair production (see below). Note that the photon induced subprocess is needed for a consistent treatment of the mass singularities in the process $gq \to t\bar{t}q$ when the t-channel photon is collinear to the quark q. It turns out that this contribution is numerically important. However, we neglect photon-initiated contributions to $\hat{\sigma}_{0;2}$ and $\hat{\sigma}_{1;2}$.

(iii) $\hat{\sigma}_{2;0}$, $\hat{\sigma}_{3;0}$. These terms are the contributions from the SM QCD "background" processes $q\bar{q}, gg \to t\bar{t}[g]$, $qg \to t\bar{t}q$ and $\bar{q}g \to t\bar{t}\,\bar{q}$ which have been computed in the late 1980s [35–38]. Furthermore, NLO calculations for heavy quark correlations [39] and $t\bar{t}$ spin correlations [40,41] are available too. The terms $\hat{\sigma}_{2;0}$ and $\hat{\sigma}_{3;0}$ are not affected by the presence of Z' or W' bosons and are readily available in many NLO + PS event generators [42–47].

(iv) $\hat{\sigma}_{2;1}$. This term represents the electroweak corrections to the QCD backgrounds. Within the SM, a gauge-invariant subset was first investigated neglecting the interferences between QCD and electroweak interactions arising from box-diagram topologies and pure photonic contributions [48] and later also including additional Higgs boson contributions arising in two-Higgs-doublet models [49]. The rest of the electroweak corrections was subsequently calculated in a series of papers and included also Z-gluon interference effects and QED corrections with real and virtual photons [50–54]. In principle, $\hat{\sigma}_{2;1}$ would also receive contributions from new Z' and W' resonances. However, these contributions are expected to give a small correction to $\hat{\sigma}_{2;1}$ and since they are highly model-dependent due to the rich structure of the scalar sector in many models we do not include them in our calculation.

(v) $\hat{\sigma}_{0;3}$. Finally, the purely electroweak term in Eq. (2) would also receive contributions from new Z' and W' resonances. It is of order $\mathcal{O}(\alpha^3)$ and parametrically suppressed compared to the other terms. We therefore do not include it in our calculation.[1]

III. NLO QCD CORRECTIONS TO ELECTROWEAK TOP-PAIR PRODUCTION

In this section, we present our new calculation of the NLO QCD corrections to electroweak top quark-pair production in the presence of heavy Z' and W' spin-one resonances where we put particular emphasis on the changes with respect to our previous calculation in Ref. [23].

A. Analysis chain

In [23], the Feynman diagrams were generated using QGRAF [57] and then translated into amplitudes using DIANA [58]. The calculation was carried out in the Feynman gauge in $D = 4 - 2\epsilon$ dimensions in order to regularize the ultraviolet (UV) and infrared divergences using FORM [59]. The loop integrals were then reduced to a

[1]Note, however, that despite the parametric suppression they have been shown to be important in the SM in a region with large top transverse momentum [55,56].

basis of three master integrals having well-known solutions [60][2] using integration-by-parts identities [61,62] in the form of the Laporta algorithm [63] as implemented in the public tool REDUZE [64,65]. Traces involving the Dirac matrix γ_5 were treated in the Larin prescription [66] by replacing $\gamma_\mu\gamma_5 = i\frac{1}{3!}\epsilon_{\mu\nu\rho\sigma}\gamma^\nu\gamma^\rho\gamma^\sigma$. We used the on shell scheme to subtract the UV divergences. Furthermore, in order to restore the Ward identities and thus preserve gauge invariance at one loop, an additional finite renormalization for vertices involving γ_5 was performed. Finally, we verified analytically that the remaining soft and soft-collinear divergences cancel in the sum of the real and virtual contributions, as a consequence of the Kinoshita-Lee-Nauenberg theorem, explicitly using the Catani-Seymour subtraction [67].[3]

We now use the public library RECOLA2 to generate the amplitudes for the models in Sec. IV. RECOLA2 is an extension of RECOLA [69] for the computation of tree and one-loop amplitudes in the Standard Model and beyond. In RECOLA, one-loop amplitudes are decomposed in terms of tensor coefficients and tensor integrals, the latter being model independent and evaluated with the help of the COLLIER tensor integral library [70]. Thus the model-dependent part only concerns the tensor coefficients and rational parts of type R_2 [71] that are being constructed with the help of a RECOLA2 model file in a recursive and numerical way. The model file used in our study has been generated using the toolchain FeynRules [72] and REPT1L [73] and is publicly available.[4] RECOLA regularizes amplitudes in dimensional regularization with space-time dimension $D = 4 - 2\epsilon$, adopting by default the COLLIER normalization for 1-loop integrals [70]. More precisely, conventional dimensional regularization is used which treats all particles and momenta in D dimensions. Similarly, the Lorentz algebra is upgraded to D-dimensions with a special treatment of γ_5, known as naïve dimensional regularization [75]. As the treatment of γ_5 is delicate in $D \neq 4$ dimensions, it can be formulated as a problem of determining the correct rational term of type R_2 which may not have a γ_5 scheme dependence or would otherwise prohibit defining (chiral) gauge symmetry of the theory in a consistent way. In naïve dimensional regularization, rational terms for amplitudes with closed fermion loops and external vector bosons are evaluated using a reading point prescription, giving up on the cyclicity of the trace. This procedure guarantees that no symmetries of the theory are being broken, at least to one-loop order. The UV renormalization is carried out in the complete on shell scheme for all particles [76]. Since in this work we start from electroweak production including QCD corrections, no further renormalization of couplings is required. Finally, with POWHEG we use the Binoth Les Houches Accord conventions [77] in which the UV renormalized 1-loop amplitude is given as the following Laurent series [78][5]:

$$\mathcal{A}_1 = C(\epsilon)\left(\frac{A_2}{\epsilon^2} + \frac{A_1}{\epsilon} + \frac{A_0}{\epsilon}\right), \qquad C(\epsilon) = \frac{4\pi}{\Gamma(1-\epsilon)}. \quad (3)$$

One final technical point that is noteworthy concerns the treatment of Goldstone bosons. RECOLA2 performs computations in Feynman gauge that requires, in general, the inclusion of Goldstone bosons which drop out whenever a Goldstone boson is attached to a massless quark line. However, for the processes under consideration and in the presence of flavor mixing this is no longer the case. For this reason we include Goldstone bosons associated to W' and Z' that mimic the interaction of the SM Goldstone bosons in such a way that the amplitudes are equivalent to a computation in unitary gauge.

B. Parton level processes

In the following, we will describe the amplitudes contributing to $\hat{\sigma}_{1;1}$, $\hat{\sigma}_{0;2}$ and $\hat{\sigma}_{1;2}$ in more detail. As already mentioned, we work in a 5-FNS including all relevant contributions with massless u, d, s, c, b (anti)quarks, gluons and photons in the initial state. Furthermore, we allow for a completely general flavor structure for the couplings of the Z' and W' bosons to the Standard Model fermions.

1. Leading-order contributions

The Born amplitudes $A_{0;1}$ contributing to the electroweak top-pair production cross section $\hat{\sigma}_{0;2} \sim |A_{0;1}|^2$ are shown in Fig. 1.

Figure 1(a) depicts in a compact form the contribution with an s-channel vector boson V_1 which can be a photon, a SM Z boson, or a new heavy Z' boson. In the previous version of PBZP we allowed only for flavor-diagonal Z' couplings with $q' = q \in \{u, d, s, c, b\}$. In this calculation we include contributions with flavor-changing couplings of the Z' boson to the quarks in the initial state ($q'\bar{q} \in \{u\bar{u}, c\bar{u}, d\bar{d}, s\bar{d}, b\bar{d}, d\bar{s}, s\bar{s}, b\bar{s}, u\bar{c}, c\bar{c}, d\bar{b}, s\bar{b}, b\bar{b}\}$). Note that the corresponding amplitudes with a charge-conjugated initial state are not shown. In the new calculation, we now also take into account the t-channel diagrams in Fig. 1(b) where the exchange boson V_2 can be a W, W' or Z' boson. Needless to say that those amplitudes in Figs. 1(a) and 1(b) having the same initial (and final) states are added coherently.

[2]These integrals are the massive tadpole, the equal-masses two-point function and the massless two-point function.

[3]Note, however, that the actual treatment of the soft and collinear divergences in PBZP was (and still is) done numerically within POWHEG using the Frixione-Kunszt-Signer subtraction [68].

[4]The model file can be found on the official website [74] under model files.

[5]This requires calling SET_DELTA_IR_RCL(0, $\pi^2/6$) in RECOLA.

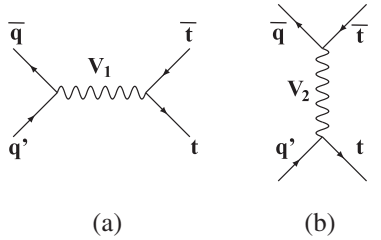

FIG. 1. Born amplitudes $A_{0;1}$ contributing to the electroweak top-pair production cross section $\hat{\sigma}_{0;2}$. (a) s-channel contribution where $V_1 \in \{\gamma, Z, Z'\}$ and $q, q' \in \{u, d, s, c, b\}$. In the case of Z' exchange we allow for flavor-changing amplitudes with $q' \neq q$ and we do not show the corresponding amplitudes with a charge-conjugated initial state. (b) t-channel contributions where $V_2 \in \{W, W', Z'\}$. All allowed amplitudes with the same initial (and final) state are added coherently.

As was discussed in [23], the diagrams in Fig. 1(a) have zero interference with the QCD amplitude $q\bar{q} \to g^* \to t\bar{t}$ since such interference terms are proportional to the vanishing color trace $\mathrm{Tr}(T^a)$. On the other hand, the t-channel diagrams in Fig. 1(b) with $q' = q$ do interfere with the QCD amplitude $q\bar{q} \to g^* \to t\bar{t}$. Thus they contribute to $\hat{\sigma}_{1;1}$ and we take them into account.

2. One-loop virtual corrections

In Fig. 2 we show the one-loop QCD corrections, $A_{1;1}$, to the diagrams in Fig. 1. They contribute to the electroweak top-pair production at $\mathcal{O}(\alpha_s\alpha^2)$ due to the interference of these diagrams with the Born amplitudes in Fig. 1: $\hat{\sigma}^{\mathrm{V}}_{1;2} \sim 2\Re[A_{0;1}A^*_{1;1}]$.

Note again, that there is no interference of the diagrams in Figs. 2(a) and 2(b) with the Born level QCD amplitude $q\bar{q} \to g^* \to t\bar{t}$, whereas the diagrams in Figs. 2(c) and 2(d) will interfere with it contributing to $\hat{\sigma}_{2;1}$. As discussed in Sec. II, we do not consider the effect of heavy new resonances on $\hat{\sigma}_{2;1}$ in this work.

In our recalculation we define the virtual corrections as the set of diagrams with no vector bosons inside the loops, effectively treating them as background fields in RECOLA2 [73,79]. The resulting QCD loop corrections constitute a gauge-invariant subset which can be seen by realizing that if either of the quark lines is replaced by an auxiliary non-color-charged conserved current (e.g., a lepton-lepton vector interaction), the so-defined virtual corrections represent not only the full QCD corrections and are thus gauge-independent, but, moreover, they do not depend on the specific form of the auxiliary conserved current. Therefore, the statement holds true for the EW production if one vetoes diagrams with a gluon exchange between the two different quark lines, i.e., excluding box corrections. In summary, we therefore include diagrams such as Figs. 2(c) and 2(d), but we omit the diagrams in Figs. 2(e)–2(h). In principle one could compute all corrections, but the renormalization of the amplitudes in Figs. 2(g) and 2(h) requires one to account for quark mixing self-energy diagrams with transitions between different flavors due to W, W' or Z' bosons in the loop. Such quark mixing in the renormalization is currently not implemented in RECOLA2/REPT1L. In the limit of a diagonal CKM matrix and including only diagonal W' and Z' couplings, we investigated in our calculation the impact of the diagrams in Figs. 2(e)–2(h) and it turns out that, in this case, their contribution is negligibly small. Since any deviation from this "diagonal" setup is additionally suppressed by the small off-diagonal couplings we expect the contributions from Figs. 2(e)–2(h) to also remain negligible in this general "non12diagonal" case.

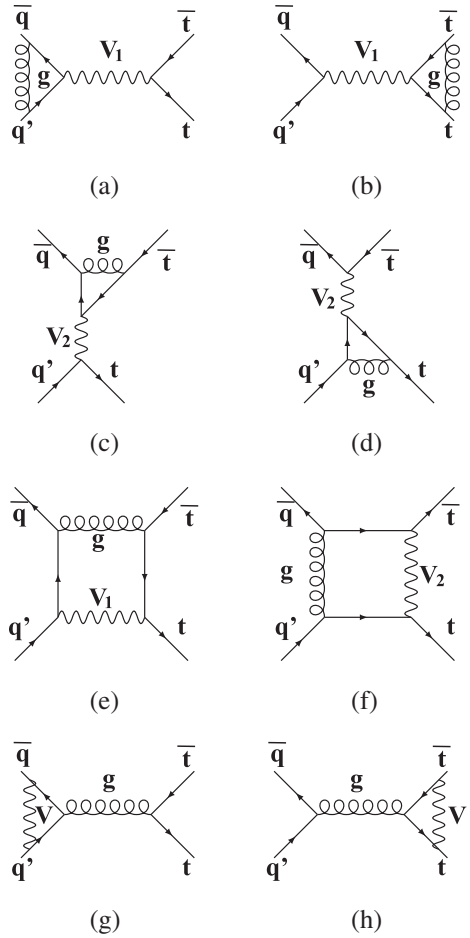

FIG. 2. One-loop QCD corrections, $A_{1;1}$, to the diagrams in Fig. 1. As before, $V_1 \in \{\gamma, Z, Z'\}$, $V_2 \in \{W, W', Z'\}$ and $V = V_1 \cup V_2$ denotes the union of V_1 and V_2.

3. Real emission corrections

The following $2 \to 3$ tree-level amplitudes, $A_{1/2;1}$, contribute to electroweak top-pair production at $\mathcal{O}(\alpha_s\alpha^2)$: (i) $q'\bar{q} \to t\bar{t}g$ (and the charge conjugated process) and (ii) $gq \to t\bar{t}q'$ (and the charge conjugated process). The corresponding Feynman diagrams are shown in Figs. 3 and 4.

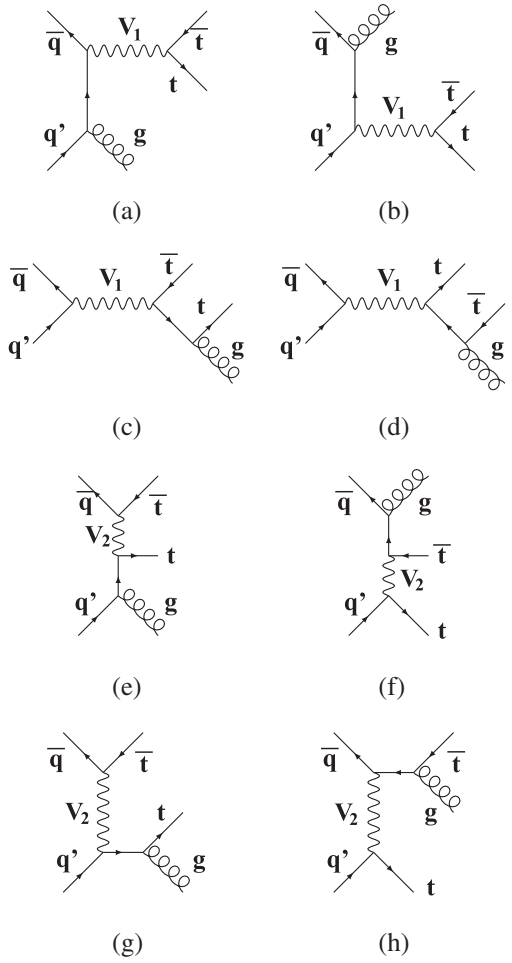

FIG. 3. Diagrams contributing to the $q'\bar{q} \to t\bar{t}g$ subprocesses at order $\mathcal{O}(\alpha_s\alpha^2)$. As in Fig. 1, $V_1 \in \{\gamma, Z, Z'\}$, $V_2 \in \{W, W', Z'\}$ and $q, q' \in \{u, d, s, c, b\}$. All allowed amplitudes with the same initial (and final) state are added coherently.

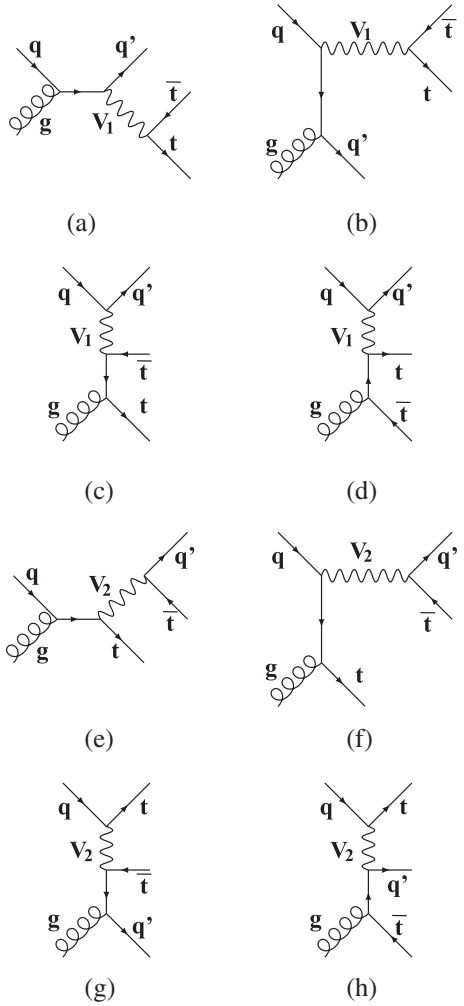

FIG. 4. Similar as in Fig. 3 but for the subprocesses $gq \to t\bar{t}q'$.

For comparison, the real emission diagrams in Figs. 4 and 5 in our previous calculation [23] are a (small) subset of the diagrams depicted in Figs. 3 and 4 in a rather compact manner.

The $q'\bar{q}$ subprocesses in Fig. 3 contain soft and collinear divergences which cancel in the sum of real and virtual cross sections as a consequence of the Kinoshita-Lee-Nauenberg theorem. As already mentioned, within POWHEG they are treated using the Frixione-Kunszt-Signer subtraction [68]. Collinear divergences are present in Figs. 3(a), 3(b), 3(e) and 3(f). On the other hand, collinear gluon emission from a top quark line leads to a finite logarithm of the top quark mass which we keep in $\hat{\sigma}$ in fixed order perturbation theory. The gq and $g\bar{q}$ channels can only have collinear singularities. While the diagrams in Figs. 4(a), 4(e), 4(f) and 4(h) are completely finite, the other diagrams in Fig. 4 contain configurations where a light quark propagator [(b),(g)] or a photon propagator [(c),(d)] can be close to its mass shell. As already discussed in [23], the fact that the collinear divergences appearing in Figs. 4(c) and 4(d) involve a photon propagator has two consequences: (i) we have to introduce a PDF for the photon inside the proton, and (ii) the corresponding underlying Born process shown in Fig. 5, $g\gamma \to t\bar{t}$, must be included in the calculation.

C. Validation

All the amplitudes with a Z' and W' obtained with RECOLA2 have been carefully checked to reproduce the SM limit, where we can rely on the correctness of RECOLA2 having been validated against many different tools such as OPENLOOPS2 [80] and MADGRAPH5_AMC@NLO [46]. Furthermore, the diagonal $\gamma/Z/Z'$ to $t\bar{t}$ amplitudes obtained

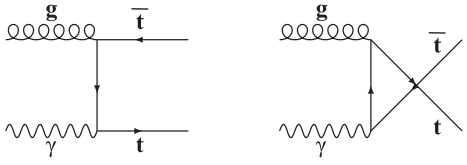

FIG. 5. Photon-induced top-pair production of $\mathcal{O}(\alpha_S\alpha)$.

with RECOLA2 have been validated at the amplitude level and at the cross section level (after implementing them in POWHEG BOX) at LO and at NLO against our old calculation. The POWHEG BOX automatically performs consistency checks on the soft and collinear structure of the amplitudes. In addition, we verified analytically the cancellation of soft-real and soft-virtual divergences of our amplitudes.

IV. MODELS

With the intention of presenting the different aspects of the new calculation we introduce three different models.

A. Sequential Standard Model

The sequential Standard Model (SSM) [81] is a toy model which copies the weak interactions of quarks and leptons by heavier versions W' and Z' of the W and Z boson, respectively. The only free parameters in this model are the masses of the new heavy gauge bosons. Due to its simplicity and convenience it is a widely used benchmark model in which LHC data are analyzed. The most stringent limits on W' and Z' masses in this model are derived from searches with dilepton final states. Assuming $\Gamma_{Z'}/m_{Z'} = 3\%$, a mass below 5.1 TeV is excluded by the ATLAS Z' search for high-mass dilepton resonances at the LHC run II with $\sqrt{S} = 13$ TeV and 139 fb^{-1} integrated luminosity (see Fig. 3 and Table 3 of [82]). The CMS search for a narrow resonance in high mass dilepton final states using data from LHC run II at $\sqrt{S} = 13$ TeV with 140 fb^{-1} integrated luminosity leads to a lower mass limit of $m_{Z'} \geq 5.15$ TeV assuming a signal width $\Gamma_{Z'}/m_{Z'} = 3\%$ (see Table 4 of [83]). For W' gauge bosons in the SSM, masses below 6.0 TeV are excluded by the ATLAS W' search with charged lepton plus missing transverse momentum final states using data from LHC run II with $\sqrt{S} = 13$ TeV and an integrated luminosity of 139 fb^{-1} [84], where $\Gamma_{W'}/m_{W'}$ varies between 2.7% at $m'_W = 150$ GeV and 3.5% above the $t\bar{b}$ threshold. The CMS W' search using LHC run II data from 2016 (not the complete run II dataset) at 35.9 fb^{-1} integrated luminosity set the lower limit on the mass of W' to 5.2 TeV [85].

B. Topcolor model

The topcolor (TC) model [86,87] can generate a large top-quark mass through the formation of a top-quark condensate. This is achieved by introducing a second strong SU(3) gauge group which couples preferentially to the third generation, while the original SU(3) gauge group couples only to the first and second generations. To block the formation of a bottom-quark condensate, a new U(1) gauge group and associated Z' boson are introduced. Different couplings of the Z' boson to the three fermion generations then define different variants of the model [88]. A popular choice with the LHC collaborations is the leptophobic TC model (also called Model IV in the reference cited above) [89], where the Z' couples only to the first and third generations of quarks and has no significant couplings to leptons. This particular choice has three parameters: the ratio of the two U(1) coupling constants, $\cot\theta_H$, which should be large to enhance the condensation of top quarks, but not bottom quarks, as well as the relative strengths f_1 and f_2 of the couplings of right-handed up- and down-type quarks with respect to those of the left-handed quarks. This model is excluded by the ATLAS search for $t\bar{t}$ resonances in fully hadronic final states in pp collisions at $\sqrt{S} = 13$ TeV and an integrated luminosity of 139 fb^{-1} for Z' masses below 3.9 and 4.7 TeV and for the decay widths of 1 and 3%, respectively [90]. At $\sqrt{S} = 13$ TeV and with an integrated luminosity of 35.9 fb^{-1}, the CMS search for resonant $t\bar{t}$ production in proton-proton collisions excludes masses up to 3.80, 5.25 and 6.65 TeV for Z' decay widths of 1, 10 and 30%, respectively [91].

C. Third family hypercharge model

The third family hypercharge model (TFHM) [1] is a minimal extension of the SM by an anomaly-free, spontaneously broken $\mathrm{U}(1)_F$ gauge symmetry. Apart from the new gauge boson (X) and a SM singlet, complex scalar field ($\Theta(x)$), needed for the spontaneous symmetry breaking of the $\mathrm{U}(1)_F$ symmetry, no new particles are introduced. The model has flavor-dependent couplings designed to explain various measurements of B meson decays ($R_K^{(\star)}$ [5,92], $\mathrm{BR}(B_s \to \mu^+\mu^-)$ [8–11], angular distributions in $B \to K^{(\star)}\mu^+\mu^-$ decays [6,7,93,94]) which are currently in tension with SM predictions. In addition, it provides an explanation of the heaviness of the third generation of SM particles and the smallness of the quark mixing. An update of the allowed parameter space (post Moriond 2019) can be found in Ref. [95]. Recently, the TFHM has been slightly modified to make it more natural in the charged lepton sector [2]. In the following we will use the original TFHMEG (Third Family Hypercharge Model example case) model from Ref. [1]. The collider phenomenology of the TFHMEG has also been studied in [96]. This model has three free parameters, the extra U(1) coupling, g_F, the angle controlling the mixing of the second and third family quarks, θ_{sb} and the Z' boson mass. The width of Z' in the TFHMEG is $\Gamma_{Z'} = \frac{5g_F^2 m_{Z'}}{36\pi}$. The Z' couplings to the quarks depend on g_F and θ_{sb} [see Eq. (2.15) in [1]]:

$$-\mathcal{L}_{X\psi} = g_F\left(\frac{1}{6}\overline{\mathbf{u_L}}\Lambda^{(u_L)}\gamma^\rho\mathbf{u_L} + \frac{1}{6}\overline{\mathbf{d_L}}\Lambda^{(d_L)}\gamma^\rho\mathbf{d_L} + \frac{2}{3}\overline{t_R}\gamma^\rho t_R - \frac{1}{3}\overline{b_R}\gamma^\rho b_R\right)Z'_\rho, \tag{4}$$

where all quark fields are in the mass eigenbasis and $\mathbf{u_L} = (u_L, c_L, t_L)^T$ and $\mathbf{d_L} = (d_L, s_L, b_L)^T$. The matrix $\Lambda^{(d_L)}$ can be found in Eq. (2.16) of Ref. [1]. It depends on θ_{sb}:

$$\Lambda^{(d_L)} = \begin{pmatrix} 0 & 0 & 0 \\ 0 & \sin^2(\theta_{sb}) & \frac{1}{2}\sin(2\theta_{sb}) \\ 0 & \frac{1}{2}\sin(2\theta_{sb}) & \cos^2(\theta_{sb}) \end{pmatrix}. \quad (5)$$

Moreover, $\Lambda^{(u_L)} = V\Lambda^{(d_L)}V^\dagger$, where V is the CKM matrix.

V. NUMERICAL RESULTS

The experimental searches for $t\bar{t}$ resonances by the ATLAS [27–29] and CMS [30–33] collaborations typically proceed as follows. After modeling the background for the reconstructed $t\bar{t}$ invariant mass distributions using data or simulations the statistical interpretation of the data is performed using two methods: (i) model-independent searches for deviations from the reconstructed invariant mass distribution ("bump hunting") and (ii) hypothesis testing for specific BSM model scenarios. In the latter case, a point in the parameter space of the model is chosen including the mass of the new hypothetical resonance, the signal is computed, and the likelihood of the "signal + background" hypothesis is computed.

It is in the spirit of the second approach, hypothesis testing,[6] that we now use our next-to-leading order calculation to obtain predictions for top-quark–pair production for the three models introduced in the preceding section: the sequential Standard Model, the topcolor model, and the third family hypercharge model. Here, our goal is not an exhaustive study of the collider phenomenology for each of these models scanning over the entire allowed parameter space, but rather to exemplify our calculation by showing results for a number of benchmark points. We will present results for the LHC at $\sqrt{S} = 14$ TeV but also for pp collisions at higher center-of-mass energies.

We will first discuss the general setup of our calculations and event selection in Secs. V A and V B before showing predictions for fiducial cross sections and NLO K factors in Sec. V C. The impact of the newly included contributions is discussed in Sec. V D, and finally the impact of the interference of the BSM signal and the SM background is studied in Sec. V E.

A. Setup and input

The theoretical description of our calculation and of the models we consider here can be found in the preceding sections. Here we describe the additional input required for the numerical computations for which the results are presented in the next few sections. This general setup and the input parameters are used by default if not stated otherwise.

We employ a top quark pole mass $m_t = 172.5$ GeV. Furthermore, the masses and widths of the weak gauge bosons are given by $m_Z = 91.1876$ GeV, $\Gamma_Z = 2.4952$ GeV, $m_W = 80.385$ GeV and $\Gamma_W = 2.085$ GeV [97]. The weak mixing angle is fixed by $\sin^2\theta_W = 1 - m_W^2/m_Z^2 = 0.222897$ and the fine-structure constant is set to $\alpha(2m_t) = 1/126.89$. We neglect the running of this coupling to higher scales. We consider quark mixing between all three families and use a unitary CKM matrix constructed using Wolfenstein parameters as in Ref. [98].

For the proton parton distribution functions (PDFs), we use the NLO lux QED set of NNPDF3.1 [99–101] as implemented in the LHAPDF library (ID = 324900) [102,103]. This set provides, in addition to the gluon and quark PDFs, a precise determination of the photon PDF inside the proton which we need for our cross section predictions. The running strong coupling $\alpha_s(\mu_R)$ is evaluated at NLO in the $\overline{\text{MS}}$ scheme and is provided together with the PDF set.[7]

For our numerical predictions in the following sections, we choose equal values for the factorization and renormalization scales, μ_F and μ_R, respectively, which we identify with the partonic center-of-mass energy: $\mu_F = \mu_R = \sqrt{\hat{s}}$. Additionally we vary μ_F and μ_R by independently multiplying the scales by factors of $\xi_R, \xi_F \in \{0.5, 1, 2\}$ discarding combinations with $\xi_F/\xi_R = 4$ or $1/4$. We combine such seven-point variations into an uncertainty band by taking the envelope of all the predictions.

We present (N)LO + PS predictions for a pp collider with a range of energies $\sqrt{S} \in \{14, 27, 50, 100\}$ TeV. We consider the SSM, TC and TFHM models and a range of Z' masses $m_{Z'} \in [2, 8]$ TeV. In the SSM we set the mass of W' equal to the mass of Z' and its mixing matrix to that of the SM W. The widths of Z' and W' bosons must then be $\Gamma_{Z'}/m_{Z'} = 3\%$, $\Gamma_{W'}/m_{W'} = 3.3\%$. The parameters of the TC model are chosen as follows: we set $f_1 = 1$ and $f_2 = 0$ and calculate $\cot\theta_H$ such that $\Gamma_{Z'}/m_{Z'} = 3.1$–3.2%. In the TFHM we set $\theta_{sb} = 0.095$, $g_F/m'_Z = 0.265$ where $m_{Z'}$ is given in TeV which implies $\Gamma_{Z'}/m_{Z'} = \{0.012, 0.028, 0.050, 0.078, 0.112, 0.152, 0.199\}$ for $m'_Z = \{2, 3, 4, 5, 6, 7, 8\}$ TeV.[8]

B. Event generation and cuts

We generate events in the Les Houches Event format [104] using POWHEG BOX with stable on-shell top quarks and require the underlying Born kinematics to satisfy a cut on the $t\bar{t}$ invariant mass $m_{t\bar{t}} \geq 0.75 m_{Z'}$, in order to enhance the signal over background ratio. We then decay both top quarks leptonically and shower the events using PYTHIA 8.244 [105]. The branching ratio of the leptonic top decay of 10.5% [98] squared is applied, unless stated otherwise.

[6] It should also be noted that model-independent searches are no longer possible once the interference between the SM and the new physics is properly taken into account as we do in this paper since a separation into "background" and "signal" is no longer well defined.

[7] Its value is fixed by the condition $\alpha_s(m_Z) = 0.118$.

[8] This benchmark point was selected from Fig. 1 in [95].

TABLE I. Total cross sections in LO for top-pair production at $\mathcal{O}(\alpha_s\alpha)$ and $\mathcal{O}(\alpha^2)$ in the SM and SSM at $\sqrt{S} = 14$ TeV. The Z'-boson mass is set to 5 TeV. For all the predictions in this table we use NLO α_S and NLO PDFs. The cross sections for $\mathcal{O}(\alpha_s^2)$ top-pair production evaluated in a similar setup can be found in Table 1 of Ref. [23].

Contribution	No cuts [fb]	$m_{t\bar{t}}$ cut [fb]	$m_{t\bar{t}}$	(pseudo)Fiducial cuts [%]
$\gamma g + g\gamma \to t\bar{t}$, $\mathcal{O}(\alpha\alpha_s)$	3700	0.0327	41.6	
$q\bar{q}' \to W \to t\bar{t}$ $\mathcal{O}(\alpha^2)$ + interf.	3220	0.0573	3.7	
$q\bar{q} \to g/W \to t\bar{t}$, $\mathcal{O}(\alpha\alpha_s)$	−1680	0.000703	37.4	
$q\bar{q} \to \gamma/Z \to t\bar{t}$, $\mathcal{O}(\alpha^2)$	510	0.00614	74.9	
$q\bar{q} \to Z' \to t\bar{t}$, $\mathcal{O}(\alpha^2)$	0.210	0.114	77.4	
$q\bar{q}' \to W' \to t\bar{t}$, $\mathcal{O}(\alpha^2)$ + interf.	0.0025	…	…	

Note that the PYTHIA decays wash out any spin correlations. We use POWHEGHOOKS to veto shower emissions harder than the POWHEG emission and disable QED showers.

We perform further event selection and bin in histograms on-the-fly using RIVET [106,107]. Events are required to have two or more charged leptons, two or more neutrinos and two or more anti-k_T [108] $R = 0.5$ jets each containing at least one b parton. All these objects have to fulfil the acceptance cuts $p_T > 25$ GeV and $|y| < 2.5$.[9] Furthermore, we combine charged leptons and neutrinos into W bosons based on their Monte Carlo truth PDG id and require each event to feature at least one such W^+ and one such W^- boson.

It is instructive to have a closer look at the size of the various leading order contributions to the EW top-pair production considered in this study, and the effects that the invariant mass and the (pseudo)fiducial cuts have on them. To that effect in Table I, we show integrated cross sections in femtobarn for the center-of-mass energy $\sqrt{S} = 14$ TeV and the Z' boson mass, $m_{Z'}$, set to 5 TeV with no cuts in the first column. The cross sections after the invariant mass cut are shown in the second column and after both invariant mass and (pseudo)fiducial cuts in the third column. Note the branching ratio of two leptonic top decays has been stripped from these predictions. We do this because the ratio of the first two columns does not depend on the decay channel and we expect the (pseudo)fiducial cuts, in this study designed for the dileptonic channel, to have a similar impact in all the other decay channels. All the contributions in the table are obtained by multiplying an amplitude by its complex conjugate except for $q\bar{q} \to g/W \to t\bar{t}$, which is calculated as $M(q\bar{q} \to W \to t\bar{t})M^*(q\bar{q} \to g \to t\bar{t}) + \text{c.c.}$. The contributions in rows 2 and 6 also contain the interference terms with the contributions in rows 4 and 5, respectively (indicated by "+interf.").

First we observe that the various SM contributions (rows 1–4) are of similar size, with the resonant production being the smallest. This must be because the Z boson resonance is below the $2m_t$ threshold. Furthermore we notice that the "interference term" in the third row is negative, which is not surprising. The invariant mass cut, see the second column, reduces all the SM contributions by roughly 5 orders of magnitude, except for the "interference term," which is reduced even more, by about 7 orders of magnitude.[10] The effect of the (pseudo)fiducial cut in the third column is expressed in terms of percentage relative to the second column. It has roughly the same impact on all the SM contributions, except for the nonresonant W boson production in the second row, in which the bulk of the cross section is in the forward regions outside the acceptance. After both cuts are applied the first two largest contributions are the photon induced and the resonant $t\bar{t}$ productions, both of which were already included in our previous calculation [23].

By design the invariant mass cut has quite a different impact on the resonant Z' production and reduces it only gently, by a factor less than two. As expected the (pseudo) fiducial cut behaves nearly the same for SM and BSM resonant productions. After both cuts are applied the Z' contribution is by far the dominant one. The cuts we designed for this study are thus more than adequate for selecting SSM $Z' \to t\bar{t}$ production with $m_{Z'} = 5$ TeV at a $\sqrt{S} = 14$ TeV LHC.

The nonresonant W' production is about two orders of magnitude smaller than the resonant one. Moreover we would expect the invariant mass and (pseudo)fiducial cuts to reduce it considerably similarly to the nonresonant W production. This contribution in the SSM and at $\sqrt{S} = 14$ TeV is thus negligible.[11] Note that this may not be the case anymore at higher collider energies.

C. Fiducial cross sections and NLO K factors

On the upper panels of Fig. 6 we show fiducial NLO + PS cross sections for the SSM, TFHM and the TC model

[9]Cuts on individual momenta of neutrinos are not realistic; however we verified that replacing these cuts by a cut on the total missing transverse momentum instead, $p_T > 30$ GeV, only has a minor impact on K factors and ratios of predictions.

[10]The invariant mass cut is a generation cut, so one does not need to worry about the numerical precision in samples without it.

[11]At the moment, this contribution cannot be calculated independently of the Z' contribution. Because it is much smaller it would require an extremely precise prediction for the Z' contribution. Thus we do not report the numbers after cuts.

versus the Z' boson mass, $m_{Z'}$, at a fixed center-of-mass energy $\sqrt{S} = 14$ TeV (left) and versus the center-of-mass energy for fixed mass $m_{Z'} = 3$ TeV (right). In the SSM the W' boson mass is always set equal to $m_{Z'}$. For comparison we also include the results for the SM[12] (gray, dashed line). The event generation setup, the invariant mass and the (pseudo)fiducial cuts are as described above. In all cases, the cross sections fall off with increasing $m_{Z'}$ and grow with increasing $\sqrt{S}$. The former is also true for the SM in which the cross section only depends on $m_{Z'}$ indirectly through the invariant mass cut.

The invariant mass cut adequately suppresses the SM background relative to the BSM signal in the SSM and in the TC model. The prediction for the TFHM model, however, can barely be distinguished from the SM background throughout the whole mass range at $\sqrt{S} = 14$ TeV. It only becomes appreciably larger than the SM at higher energies, where its ratio over the SM is roughly 1.13 at $\sqrt{S} = 100$ TeV. Adopting a tighter invariant mass cut would be advised for the TFHM, for example $m_{Z'} - \Gamma_{Z'} < m_{t\bar{t}} < m_{Z'} + \Gamma_{Z'}$.

The NLO + PS over LO + PS K factors, shown on the lower panels of Fig. 6, are moderate to large and grow with Z' boson mass up to ∼40% in the TC model and up to ∼60% in the SSM. In the absence of BSM effects, this ratio effectively measures the dependence of higher order corrections on the partonic center-of-mass energy. Between 2 and 4 TeV this ratio is fairly flat but then quickly grows, surpassing 60% at 8 TeV. As expected, the K factors in the TFHM closely follow those of the SM.

Conversely, the K factors follow the opposite trend versus $\sqrt{S}$ and eventually almost all drop below one for $m_{Z'} = 3$ TeV. It would be interesting to see whether the higher order corrections for larger Z' masses follow a similar pattern.

Higher order corrections are often included in experimental searches in terms of a constant K factor. While this is more or less well justified for a range of Z' masses between 2 and 5 TeV, the corrections more than double when this range is extended to 2–8 TeV. It may thus be desirable to abandon this crude approximation in high luminosity or high energy searches where we expect the reach to extend considerably.

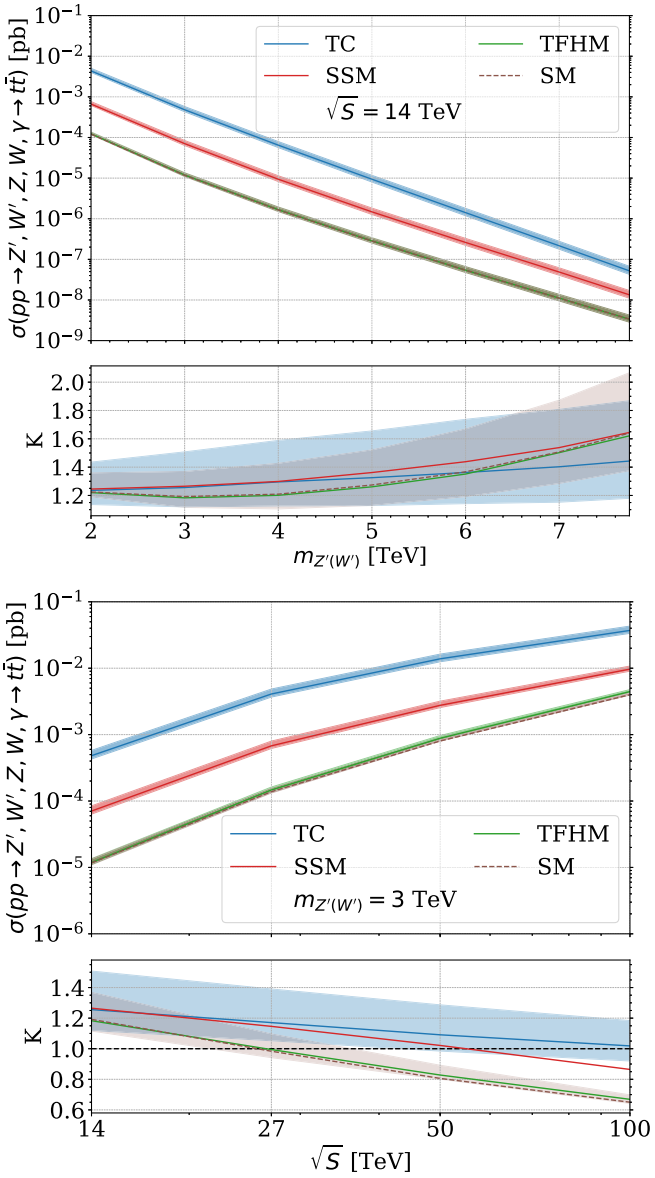

FIG. 6. Fiducial cross sections for EW $t\bar{t}$ production in the SM, SSM, TC and TFHM with an invariant mass cut $m_{t\bar{t}} \geq 0.75 m_{Z'}$ and our event selection cuts at NLO + PS (upper panels), and as ratio to LO + PS (lower panels). In the SSM $m_{W'} = m_{Z'}$. The bands represent perturbative uncertainty due to seven-point variation of μ_F and μ_R. Left panel: cross sections at $\sqrt{S} = 14$ TeV as a function of $m_{Z'}$. Right panel: cross sections at $m_{Z'} = 3$ TeV as a function of $\sqrt{S}$.

D. Impact of nonresonant contributions

A new feature of our calculation is that we include nonresonant contributions with t-channel W, W' and Z' exchange. We study their impact here.

In Fig. 7 we show the ratio of predictions for cross sections for EW $t\bar{t}$ production in the SSM obtained using our new version of PBZP over the old one of Ref. [23]. The left panel shows this ratio as a function of $m_{Z'} = m_{W'}$ at $\sqrt{S} = 14$ TeV, the right panel as a function of $\sqrt{S}$ at $m_{Z'} = m_{W'} = 3$ TeV. The cross sections have been calculated with an invariant mass cut $m_{t\bar{t}} \geq 0.75 m_{Z'}$ and with (red lines) and without (blue lines) (pseudo)fiducial cuts, at NLO + PS (solid lines) and LO + PS (dashed lines).

The ratio of our predictions at $\sqrt{S} = 14$ TeV is roughly between 1.2 and 1.5 when (pseudo)fiducial cuts are not considered. The reason behind it is the new nonresonant contribution, due to the SM t-channel process $q\bar{q}' \to W \to t\bar{t}$,

[12]Note that this does not include the QCD contribution.

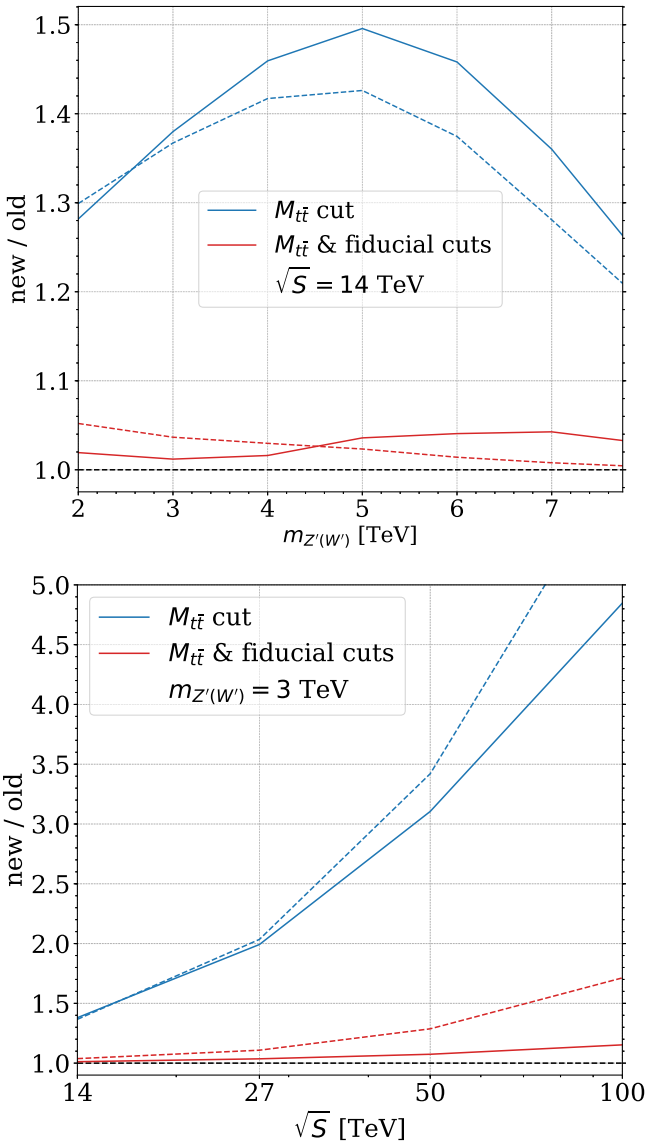

FIG. 7. The ratio of cross sections for EW $t\bar{t}$ production in the SSM in the new calculation, including t-channel W and W' exchange contributions, over the old calculation, without these contributions, at NLO + PS (solid lines) and LO + PS (dashed lines). The cross sections have been calculated with an invariant mass cut $m_{t\bar{t}} \geq 0.75 m_{Z'}$ and with (red lines) and without (blue lines) (pseudo)fiducial cuts. Left panel: cross section ratio at $\sqrt{S} = 14$ TeV as a function of $m_{Z'} = m_{W'}$. Right panel: cross section ratio at $m_{Z'} = m_{W'} = 3$ TeV as a function of $\sqrt{S}$.

not falling off with the invariant mass as fast as the resonant one. This behavior was already observed in Table I, where this process contributes less than the resonant Z' production after the invariant mass cut but is still roughly of the same order of magnitude. In this respect the $q\bar{q}' \to W \to t\bar{t}$ t-channel process behaves similarly to the $\gamma g + g\gamma \to t\bar{t}$ process, which was already included in our old calculation. The situation worsens as the center-of-mass energy is increased, the value of the ratio reaching almost 5 at $\sqrt{S} = 100$ TeV.

Once the (pseudo)fiducial cuts are switched on, the new contributions are reduced considerably and the ratio of the "new/old" predictions drops down to roughly between 1.0 and 1.05 across the whole mass range at $\sqrt{S} = 14$ TeV and between 1.0 and 1.2 across the whole $\sqrt{S}$ range at fixed mass $m_{Z'} = m_{W'} = 3$. This is simply because the bulk of the high invariant mass cross section for the $q\bar{q}' \to W \to t\bar{t}$ process lives in the forward region. In this respect the $q\bar{q}' \to W \to t\bar{t}$ process is quite dissimilar to the $\gamma g + g\gamma \to t\bar{t}$ process.

QCD corrections do not change this picture appreciably, but we note that the corrections to this ratio can be considerable at high center-of-mass energies, over 50%. Our new calculation thus confirms our previous predictions for the SSM at $\sqrt{S} = 14$ TeV, while at the same time it offers a much more sophisticated description of the interplay of various contributions that enter electroweak top-pair production. This interplay may become very important for Z's with weaker couplings and will certainly become important at higher collider energies.

E. Signal-background interference

Interferences between the BSM signal and the SM background are routinely neglected even in the most recent experimental searches. The argument is that interferences mostly affect the shapes of resonance bumps, which "bump-hunting" is largely insensitive to. Consequently, experimental analyses work with the SM only and the SM + BSM hypotheses, where the latter is a "naïve" sum of the signal and the background.

While interference effects are expected to integrate out in total cross sections, they may no longer be negligible once invariant mass and (pseudo)fiducial cuts are considered. In this section we explore interference effects by studying ratios of the fiducial cross sections for EW $t\bar{t}$ production obtained either using the full process $pp \to \gamma, Z, Z', W' \to t\bar{t}$ or by summing the SM background process $pp \to \gamma, Z \to t\bar{t}$ and the SSM signal $pp \to Z', W' \to t\bar{t}$. Both sets of predictions will include all the contributions to the EW top-pair production considered in our new calculation with one exception: those obtained by summing the SM background and the BSM signal will not include any of the interference terms $\{\gamma, Z, W\} \times \{Z', W'\}$.

This ratio of the cross sections with the interference terms over the ones without them is shown in Fig. 8 as a function of $m_{Z'}$ on the left and as a function of $\sqrt{S}$ on the right. As in the previous section, the predictions with the invariant mass cut are shown in blue, the predictions with both the invariant mass and the (pseudo)fiducial cuts in red; the NLO + PS predictions are plotted with solid lines, while LO + PS are the ones with dashed lines. We find that the interference reduces the cross section at $\sqrt{S} = 14$ TeV and has a relatively steep profile versus $m_{Z'}$ at LO: a few percent for the light Z's to well over 20% for the heavy ones. The size of the interference effects seem rather flat as

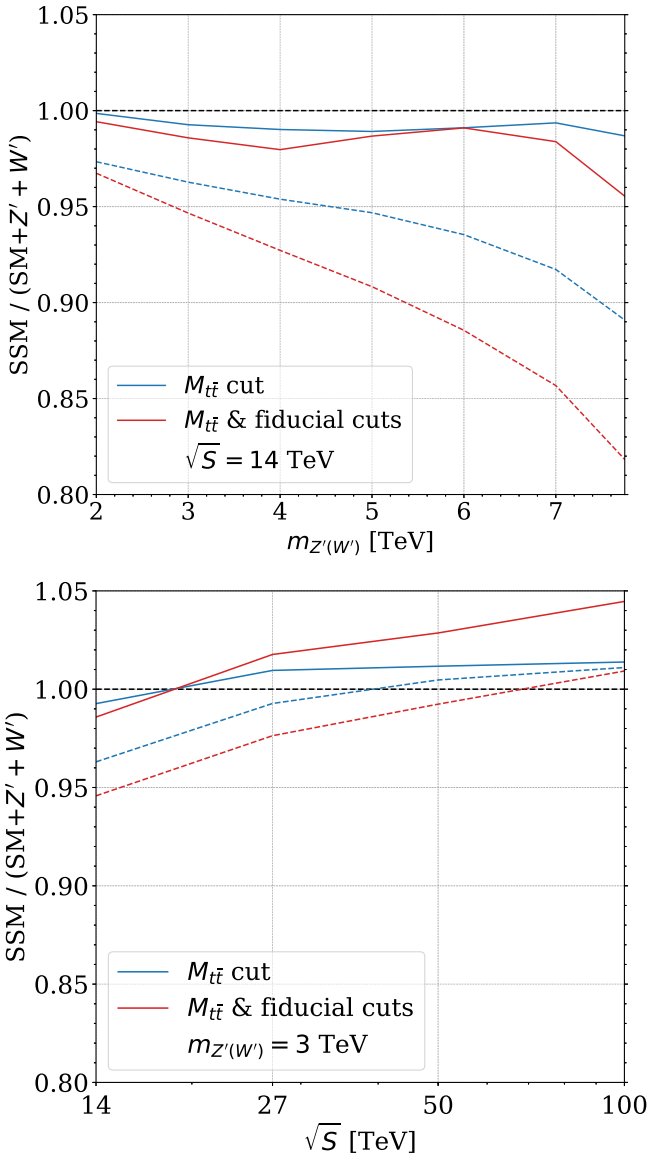

FIG. 8. The ratio of the cross section for EW $t\bar{t}$ production in the SSM with and without the interference terms between the SM and the Z', W' contributions at NLO + PS (solid) and LO + PS (dashed). The cross sections have been calculated with an invariant mass cut $m_{t\bar{t}} \geq 0.75 m_{Z'}$ and with (red line) and without (blue line) (pseudo)fiducial cuts. Left panel: cross section ratio at $\sqrt{S} = 14$ TeV as a function of $m_{Z'} = m_{W'}$. Right panel: cross section ratio at $m_{Z'} = m_{W'} = 3$ TeV as a function of $\sqrt{S}$.

a function of $\sqrt{S}$ for fixed $m_{Z'} = m_{W'} = 3$ TeV in comparison. We also observe that the interference effects tend to be pronounced by the (pseudo)fiducial cuts, while the higher order corrections rather stabilize them.

Note that these conclusions may not generalize, as we expect the interference effects to strongly depend on the BSM scenario and on the position of the invariant mass cut. In view of their potentially large size, however, we advocate they be considered in experimental searches.

VI. SUMMARY AND CONCLUSIONS

We extended and improved upon our previous calculation of electroweak top-quark pair hadroproduction in extensions of the Standard Model with extra heavy neutral and charged spin-1 resonances. In particular, we now allow for flavor-non-diagonal Z' couplings in order to accommodate a wider class of heavy resonance models including models which have been brought forward to explain the anomalies in B decays. We now also take into account nonresonant production in the SM and beyond, including the contributions with t-channel W, W' and Z' bosons. Compared to our previous work, the entire chain of tools used for the calculation changed; all amplitudes are now generated using the RECOLA2 package. Our calculation is one of the first to use RECOLA2 for a BSM calculation. As in our previous work, we included NLO QCD corrections and consistently matched them to parton showers with the POWHEG method fully taking into account the interference effects between SM and new physics amplitudes. This study paves the way for a similar upcoming calculation for the $t\bar{b}$ final state.

As a first application, we presented numerical results for $t\bar{t}$ cross sections at hadron colliders with a center-of-mass energy up to 100 TeV for three models, the sequential Standard Model, the topcolor model, as well as the third family hypercharge model leaving a more detailed analysis including comparisons with LHC data for a future study. We discussed the effect of cuts on the signal over background ratio and present K factors which turned out to increase considerably as a function of the heavy resonance mass. The impact of the new contributions was shown to be modest at 14 TeV if suitable cuts are applied. However, they are expected to become sizable at a future circular collider operated at 100 TeV. At such energies it would be interesting to compare our predictions with results obtained in a 6-flavor number scheme including parton densities for the top quark and the weak bosons of the Standard Model.

ACKNOWLEDGMENTS

The work of T. J. was in part supported by the DFG under Grant No. 396021762—TRR257 and in part by the SNSF under Contracts No. BSCGI0-157722 and No. CRSII2-160814. The work of M. M. A. and I. S. was supported in part by the IN2P3 master project Théorie BSMGA. M. M. A. is thankful for the hospitality of the Physics Institute of University of Zürich where part of this work was performed. J.-N. L. was supported by the SNSF under Contract No. BSCGI0-157722. This work has also been supported by the BMBF under Contract No. 05H18PMCC1.

[1] B. C. Allanach and J. Davighi, Third family hypercharge model for $R_{K^{(*)}}$ and aspects of the fermion mass problem, J. High Energy Phys. 12 (2018) 075.

[2] B. C. Allanach and J. Davighi, Naturalising the third family hypercharge model for neutral current B-anomalies, Eur. Phys. J. C **79**, 908 (2019).

[3] A. Crivellin, G. D'Ambrosio, and J. Heeck, Explaining $h \to \mu^{\pm}\tau^{\mp}$, $B \to K^{*}\mu^{+}\mu^{-}$ and $B \to K\mu^{+}\mu^{-}/B \to Ke^{+}e^{-}$ in a Two-Higgs-Doublet Model with Gauged $L_{\mu} - L_{\tau}$, Phys. Rev. Lett. **114**, 151801 (2015).

[4] A. Crivellin, G. D'Ambrosio, and J. Heeck, Addressing the LHC flavor anomalies with horizontal gauge symmetries, Phys. Rev. D **91**, 075006 (2015).

[5] R. Aaij *et al.* (LHCb Collaboration), Test of lepton universality with $B^0 \to K^{*0}\ell^{+}\ell^{-}$ decays, J. High Energy Phys. 08 (2017) 055.

[6] R. Aaij *et al.* (LHCb Collaboration), Angular analysis of the $B^0 \to K^{*0}\mu^{+}\mu^{-}$ decay using 3 fb^{-1} of integrated luminosity, J. High Energy Phys. 02 (2016) 104.

[7] R. Aaij *et al.* (LHCb Collaboration), Measurement of Form-Factor-Independent Observables in the Decay $B^0 \to K^{*0}\mu^{+}\mu^{-}$, Phys. Rev. Lett. **111**, 191801 (2013).

[8] R. Aaij *et al.* (LHCb Collaboration), Measurement of the $B_s^0 \to \mu^{+}\mu^{-}$ Branching Fraction and Effective Lifetime and Search for $B^0 \to \mu^{+}\mu^{-}$ Decays, Phys. Rev. Lett. **118**, 191801 (2017).

[9] M. Aaboud *et al.* (ATLAS Collaboration), Study of the rare decays of B_s^0 and B^0 mesons into muon pairs using data collected during 2015 and 2016 with the ATLAS detector, J. High Energy Phys. 04 (2019) 098.

[10] V. Khachatryan *et al.* (CMS, LHCb Collaboration), Observation of the rare $B_s^0 \to \mu^{+}\mu^{-}$ decay from the combined analysis of CMS and LHCb data, Nature (London) **522**, 68 (2015).

[11] S. Chatrchyan *et al.* (CMS Collaboration), Measurement of the $B_s^0 \to \mu^{+}\mu^{-}$ Branching Fraction and Search for $B^0 \to \mu^{+}\mu^{-}$ with the CMS Experiment, Phys. Rev. Lett. **111**, 101804 (2013).

[12] C. Bobeth, M. Chrzaszcz, D. van Dyk, and J. Virto, Long-distance effects in $B \to K^{*}\ell\ell$ from analyticity, Eur. Phys. J. C **78**, 451 (2018).

[13] V. Khachatryan *et al.* (CMS Collaboration), Angular analysis of the decay $B^0 \to K^{*0}\mu^{+}\mu^{-}$ from pp collisions at $\sqrt{s} = 8$ TeV, Phys. Lett. B **753**, 424 (2016).

[14] M. Algueró, B. Capdevila, A. Crivellin, S. Descotes-Genon, P. Masjuan, J. Matias, M. N. Brunet, and J. Virto, Emerging patterns of new physics with and without lepton flavor universal contributions, Eur. Phys. J. C **79**, 714 (2019); Eur. Phys. J. C **80**, 511(A) (2020).

[15] E. Accomando, D. Becciolini, A. Belyaev, S. Moretti, and C. Shepherd-Themistocleous, Z' at the LHC: Interference and finite width effects in Drell-Yan, J. High Energy Phys. 10 (2013) 153.

[16] E. Accomando, F. Coradeschi, T. Cridge, J. Fiaschi, F. Hautmann, S. Moretti, C. Shepherd-Themistocleous, and C. Voisey, Production of Z'-boson resonances with large width at the LHC, Phys. Lett. B **803**, 135293 (2020).

[17] B. Fuks, M. Klasen, F. Ledroit, Q. Li, and J. Morel, Precision predictions for Z'—production at the CERN LHC: QCD matrix elements, parton showers, and joint resummation, Nucl. Phys. **B797**, 322 (2008).

[18] B. Fuks, M. Klasen, D. R. Lamprea, and M. Rothering, Precision predictions for electroweak superpartner production at hadron colliders with Resummino, Eur. Phys. J. C **73**, 2480 (2013).

[19] T. Jezo, M. Klasen, D. R. Lamprea, F. Lyonnet, and I. Schienbein, NLO + NLL limits on W' and Z' gauge boson masses in general extensions of the standard model, J. High Energy Phys. 12 (2014) 092.

[20] M. Klasen, F. Lyonnet, and F. S. Queiroz, NLO + NLL collider bounds, Dirac fermion and scalar dark matter in the B–L model, Eur. Phys. J. C **77**, 348 (2017).

[21] X. C. Vidal *et al.*, *Report from Working Group 3: Beyond the Standard Model physics at the HL-LHC and HE-LHC* (CERN, 2019), Vol. 7, pp. 585–865, ISBN 978-92-9083-549-3.

[22] L. Basso, K. Mimasu, and S. Moretti, Z' signals in polarised top-antitop final states, J. High Energy Phys. 09 (2012) 024.

[23] R. Bonciani, T. Jezo, M. Klasen, F. Lyonnet, and I. Schienbein, Electroweak top-quark pair production at the LHC with Z' bosons to NLO QCD in POWHEG, J. High Energy Phys. 02 (2016) 141.

[24] P. Nason, A new method for combining NLO QCD with shower Monte Carlo algorithms, J. High Energy Phys. 11 (2004) 040.

[25] S. Frixione, P. Nason, and C. Oleari, Matching NLO QCD computations with parton shower simulations: The POWHEG method, J. High Energy Phys. 11 (2007) 070.

[26] S. Alioli, P. Nason, C. Oleari, and E. Re, A general framework for implementing NLO calculations in shower Monte Carlo programs: The POWHEG BOX, J. High Energy Phys. 06 (2010) 043.

[27] M. Aaboud *et al.* (ATLAS Collaboration), Search for heavy particles decaying into top-quark pairs using lepton-plus-jets events in proton–proton collisions at $\sqrt{s} = 13$ TeV with the ATLAS detector, Eur. Phys. J. C **78**, 565 (2018).

[28] M. Aaboud *et al.* (ATLAS Collaboration), Search for heavy particles decaying into a top-quark pair in the fully hadronic final state in pp collisions at $\sqrt{s} =$ 13 TeV with the ATLAS detector, Phys. Rev. D **99**, 092004 (2019).

[29] G. Aad *et al.* (ATLAS Collaboration), Search for $t\bar{t}$ resonances in fully hadronic final states in pp collisions at $\sqrt{s} = 13$ TeV with the ATLAS detector, J. High Energy Phys. 10 (2020) 061.

[30] CMS Collaboration, Search for $\mathrm{t\bar{t}}$ resonances in boosted semileptonic final states in pp collisions at $\sqrt{s} = 13$ TeV, CERN Report No. CMS-PAS-B2G-15-002, 2016.

[31] CMS Collaboration, Search for top quark-antiquark resonances in the all-hadronic final state at $\sqrt{s} = 13$ TeV, CERN Report No. CMS-PAS-B2G-15-003, 2016.

[32] A. M. Sirunyan *et al.* (CMS Collaboration), Search for $\mathrm{t\bar{t}}$ resonances in highly boosted lepton + jets and fully hadronic final states in proton-proton collisions at $\sqrt{s} = 13$ TeV, J. High Energy Phys. 07 (2017) 001.

[33] CMS Collaboration, Estimated sensitivity for new particle searches at the HL-LHC, Report No. CMS-PAS-FTR-16-005, 2017.

[34] A. Denner, J.-N. Lang, and S. Uccirati, Recola2: REcursive computation of one-loop amplitudes 2, Comput. Phys. Commun. **224**, 346 (2018).

[35] P. Nason, S. Dawson, and R. K. Ellis, The total cross-section for the production of heavy quarks in hadronic collisions, Nucl. Phys. **B303**, 607 (1988).

[36] P. Nason, S. Dawson, and R. K. Ellis, The one particle inclusive differential cross-section for heavy quark production in hadronic collisions, Nucl. Phys. **B327**, 49 (1989).

[37] W. Beenakker, H. Kuijf, W. van Neerven, and J. Smith, QCD corrections to heavy quark production in p anti-p collisions, Phys. Rev. D **40**, 54 (1989).

[38] W. Beenakker, W. van Neerven, R. Meng, G. Schuler, and J. Smith, QCD corrections to heavy quark production in hadron hadron collisions, Nucl. Phys. **B351**, 507 (1991).

[39] M. L. Mangano, P. Nason, and G. Ridolfi, Heavy quark correlations in hadron collisions at next-to-leading order, Nucl. Phys. **B373**, 295 (1992).

[40] W. Bernreuther, A. Brandenburg, Z. Si, and P. Uwer, Top Quark Spin Correlations at Hadron Colliders: Predictions at Next-to-Leading Order QCD, Phys. Rev. Lett. **87**, 242002 (2001).

[41] W. Bernreuther, A. Brandenburg, Z. Si, and P. Uwer, Top quark pair production and decay at hadron colliders, Nucl. Phys. **B690**, 81 (2004).

[42] S. Frixione, P. Nason, and G. Ridolfi, A positive-weight next-to-leading-order Monte Carlo for heavy flavor hadroproduction, J. High Energy Phys. 09 (2007) 126.

[43] J. M. Campbell, R. K. Ellis, P. Nason, and E. Re, Top-pair production and decay at NLO matched with parton showers, J. High Energy Phys. 04 (2015) 114.

[44] T. Ježo, J. M. Lindert, P. Nason, C. Oleari, and S. Pozzorini, An NLO + PS generator for $t\bar{t}$ and Wt production and decay including non-resonant and interference effects, Eur. Phys. J. C **76**, 691 (2016).

[45] T. Gleisberg, S. Hoeche, F. Krauss, M. Schonherr, S. Schumann, F. Siegert, and J. Winter, Event generation with SHERPA 1.1, J. High Energy Phys. 02 (2009) 007.

[46] J. Alwall, R. Frederix, S. Frixione, V. Hirschi, F. Maltoni, O. Mattelaer, H.-S. Shao, T. Stelzer, P. Torrielli, and M. Zaro, The automated computation of tree-level and next-to-leading order differential cross sections, and their matching to parton shower simulations, J. High Energy Phys. 07 (2014) 079.

[47] J. Bellm *et al.*, Herwig 7.0/Herwig++ 3.0 release note, Eur. Phys. J. C **76**, 196 (2016).

[48] W. Beenakker, A. Denner, W. Hollik, R. Mertig, T. Sack, and D. Wackeroth, Electroweak one loop contributions to top pair production in hadron colliders, Nucl. Phys. **B411**, 343 (1994).

[49] C. Kao and D. Wackeroth, Parity violating asymmetries in top pair production at hadron colliders, Phys. Rev. D **61**, 055009 (2000).

[50] J. H. Kuhn, A. Scharf, and P. Uwer, Electroweak corrections to top-quark pair production in quark-antiquark annihilation, Eur. Phys. J. C **45**, 139 (2006).

[51] S. Moretti, M. Nolten, and D. Ross, Weak corrections to gluon-induced top-antitop hadro-production, Phys. Lett. B **639**, 513 (2006).

[52] W. Bernreuther, M. Fuecker, and Z. Si, Mixed QCD and weak corrections to top quark pair production at hadron colliders, Phys. Lett. B **633**, 54 (2006).

[53] W. Bernreuther, M. Fuecker, and Z.-G. Si, Weak interaction corrections to hadronic top quark pair production, Phys. Rev. D **74**, 113005 (2006).

[54] W. Hollik and M. Kollar, NLO QED contributions to top-pair production at hadron collider, Phys. Rev. D **77**, 014008 (2008).

[55] D. Pagani, I. Tsinikos, and M. Zaro, The impact of the photon PDF and electroweak corrections on $t\bar{t}$ distributions, Eur. Phys. J. C **76**, 479 (2016).

[56] C. Gütschow, J. M. Lindert, and M. Schönherr, Multi-jet merged top-pair production including electroweak corrections, Eur. Phys. J. C **78**, 317 (2018).

[57] P. Nogueira, Automatic Feynman graph generation, J. Comput. Phys. **105**, 279 (1993).

[58] M. Tentyukov and J. Fleischer, A Feynman diagram analyzer DIANA, Comput. Phys. Commun. **132**, 124 (2000).

[59] J. Vermaseren, New features of FORM, arXiv:math-ph/0010025.

[60] G. 't Hooft and M. Veltman, Scalar one loop integrals, Nucl. Phys. **B153**, 365 (1979).

[61] F. Tkachov, A theorem on analytical calculability of four loop renormalization group functions, Phys. Lett. **100B**, 65 (1981).

[62] K. Chetyrkin and F. Tkachov, Integration by parts: The algorithm to calculate beta functions in 4 loops, Nucl. Phys. **B192**, 159 (1981).

[63] S. Laporta, High precision calculation of multiloop Feynman integrals by difference equations, Int. J. Mod. Phys. A **15**, 5087 (2000).

[64] C. Studerus, Reduze—Feynman integral reduction in C++, Comput. Phys. Commun. **181**, 1293 (2010).

[65] A. von Manteuffel and C. Studerus, Reduze 2—distributed Feynman integral reduction, arXiv:1201.4330.

[66] S. A. Larin, The renormalization of the axial anomaly in dimensional regularization, Phys. Lett. B **303**, 113 (1993).

[67] S. Catani, S. Dittmaier, M. H. Seymour, and Z. Trocsanyi, The dipole formalism for next-to-leading order QCD calculations with massive partons, Nucl. Phys. **B627**, 189 (2002).

[68] S. Frixione, Z. Kunszt, and A. Signer, Three jet cross-sections to next-to-leading order, Nucl. Phys. **B467**, 399 (1996).

[69] S. Actis, A. Denner, L. Hofer, J.-N. Lang, A. Scharf, and S. Uccirati, RECOLA: REcursive computation of one-loop amplitudes, Comput. Phys. Commun. **214**, 140 (2017).

[70] A. Denner, S. Dittmaier, and L. Hofer, Collier: A fortran-based complex one-loop library in extended regularizations, Comput. Phys. Commun. **212**, 220 (2017).

[71] G. Ossola, C. G. Papadopoulos, and R. Pittau, On the rational terms of the one-loop amplitudes, J. High Energy Phys. 05 (2008) 004.

[72] A. Alloul, N. D. Christensen, C. Degrande, C. Duhr, and B. Fuks, FeynRules 2.0—A complete toolbox for tree-level phenomenology, Comput. Phys. Commun. **185**, 2250 (2014).

[73] A. Denner, J.-N. Lang, and S. Uccirati, NLO electroweak corrections in extended Higgs Sectors with RECOLA2, J. High Energy Phys. 07 (2017) 087.

[74] https://recola.hepforge.org/

[75] A. Denner and S. Dittmaier, Electroweak radiative corrections for collider physics, Phys. Rep. **864**, 1 (2020).

[76] A. Denner, Techniques for calculation of electroweak radiative corrections at the one loop level and results for W physics at LEP-200, Fortschr. Phys. **41**, 307 (1993).

[77] S. Alioli *et al.*, Update of the Binoth Les Houches Accord for a standard interface between Monte Carlo tools and one-loop programs, Comput. Phys. Commun. **185**, 560 (2014).

[78] T. Binoth *et al.*, A proposal for a standard interface between Monte Carlo tools and one-loop programs, Comput. Phys. Commun. **181**, 1612 (2010).

[79] A. Denner, G. Weiglein, and S. Dittmaier, Application of the background field method to the electroweak standard model, Nucl. Phys. **B440**, 95 (1995).

[80] F. Buccioni, J.-N. Lang, J. M. Lindert, P. Maierhöfer, S. Pozzorini, H. Zhang, and M. F. Zoller, OpenLoops 2, Eur. Phys. J. C **79**, 866 (2019).

[81] G. Altarelli, B. Mele, and M. Ruiz-Altaba, Searching for new heavy vector bosons in $p\bar{p}$ colliders, Z. Phys. C **45**, 109 (1989); , Erratum, Z. Phys. C **47**, 676 (1990).

[82] G. Aad *et al.* (ATLAS Collaboration), Search for high-mass dilepton resonances using 139 fb^{-1} of pp collision data collected at $\sqrt{s} = 13$ TeV with the ATLAS detector, Phys. Lett. B **796**, 68 (2019).

[83] CMS Collaboration, Search for a narrow resonance in high-mass dilepton final states in proton-proton collisions using 140 fb^{-1} of data at $\sqrt{s} = 13$ TeV, No. CMS-PAS-EXO-19-019.

[84] G. Aad *et al.* (ATLAS Collaboration), Search for a heavy charged boson in events with a charged lepton and missing transverse momentum from pp collisions at $\sqrt{s} = 13$ TeV with the ATLAS detector, Phys. Rev. D **100**, 052013 (2019).

[85] A. M. Sirunyan *et al.* (CMS Collaboration), Search for high-mass resonances in final states with a lepton and missing transverse momentum at $\sqrt{s} = 13$ TeV, J. High Energy Phys. 06 (2018) 128.

[86] C. T. Hill, Topcolor: Top quark condenzation in a gauge extension of the standard model, Phys. Lett. B **266**, 419 (1991).

[87] C. T. Hill, Topcolor assisted technicolor, Phys. Lett. B **345**, 483 (1995).

[88] R. M. Harris, C. T. Hill, and S. J. Parke, Cross-section for topcolor Z'_t decaying to $t\bar{t}$, arXiv:hep-ph/9911288.

[89] R. M. Harris and S. Jain, Cross sections for leptophobic topcolor Z' decaying to top-antitop, Eur. Phys. J. C **72**, 2072 (2012).

[90] G. Aad *et al.* (ATLAS Collaboration), Search for $t\bar{t}$ resonances in fully hadronic final states in pp collisions at $\sqrt{s} = 13$ TeV with the ATLAS detector, J. High Energy Phys. 10 (2020) 061.

[91] A. M. Sirunyan *et al.* (CMS Collaboration), Search for resonant $\mathrm{t\bar{t}}$ production in proton-proton collisions at $\sqrt{s} = 13$ TeV, J. High Energy Phys. 04 (2019) 031.

[92] R. Aaij *et al.* (LHCb Collaboration), Search for Lepton-Universality Violation in $B^+ \to K^+\ell^+\ell^-$ Decays, Phys. Rev. Lett. **122**, 191801 (2019).

[93] ATLAS Collaboration, T. A. collaboration, Angular analysis of $B^0_d \to K^*\mu^+\mu^-$ decays in pp collisions at $\sqrt{s} =$ 8 TeV with the ATLAS detector, Report No. ATLAS-CONF-2017-023.

[94] CMS Collaboration, Measurement of angular parameters from the decay $\mathrm{B}^0 \to \mathrm{K}^{*0}\mu^+\mu^-$ in proton-proton collisions at $\sqrt{s} = 8$ TeV, Phys. Lett. B **781**, 517 (2018).

[95] J. Davighi, Connecting neutral current B anomalies with the heaviness of the third family, in *54th Rencontres de Moriond on QCD and High Energy Interactions (Moriond QCD 2019) La Thuile, Italy, March 23-30, 2019* (ARISF, 2019), ISBN 9791096879113.

[96] B. C. Allanach, J. M. Butterworth, and T. Corbett, Collider constraints on Z' models for neutral current B-anomalies, J. High Energy Phys. 08 (2019) 106.

[97] C. Patrignani *et al.* (Particle Data Group), Review of particle physics, Chin. Phys. C **40**, 100001 (2016).

[98] P. Zyla *et al.* (Particle Data Group), Review of particle physics, Prog. Theor. Exp. Phys. **2020**, 083C01 (2020).

[99] V. Bertone, S. Carrazza, N. P. Hartland, and J. Rojo (NNPDF Collaboration), Illuminating the photon content of the proton within a global PDF analysis, SciPost Phys. **5**, 008 (2018).

[100] A. Manohar, P. Nason, G. P. Salam, and G. Zanderighi, How Bright is the Proton? A Precise Determination of the Photon Parton Distribution Function, Phys. Rev. Lett. **117**, 242002 (2016).

[101] A. V. Manohar, P. Nason, G. P. Salam, and G. Zanderighi, The photon content of the proton, J. High Energy Phys. 12 (2017) 046.

[102] A. Buckley, J. Ferrando, S. Lloyd, K. Nordström, B. Page, M. Rüfenacht, M. Schönherr, and G. Watt, LHAPDF6: Parton density access in the LHC precision era, Eur. Phys. J. C **75**, 132 (2015).

[103] J. Andersen *et al.*, Les Houches 2013: Physics at TeV colliders: Standard model working group report, arXiv: 1405.1067.

[104] J. Alwall *et al.*, A standard format for Les Houches event files, Comput. Phys. Commun. **176**, 300 (2007).

[105] T. Sjostrand, S. Mrenna, and P. Z. Skands, A brief introduction to PYTHIA 8.1, Comput. Phys. Commun. **178**, 852 (2008).

[106] A. Buckley, J. Butterworth, L. Lonnblad, D. Grellscheid, H. Hoeth, J. Monk, H. Schulz, and F. Siegert, Rivet user manual, Comput. Phys. Commun. **184**, 2803 (2013).

[107] C. Bierlich *et al.*, Robust independent validation of experiment and theory: Rivet version 3, SciPost Phys. **8**, 026 (2020).

[108] M. Cacciari, G. P. Salam, and G. Soyez, The anti-k_t jet clustering algorithm, J. High Energy Phys. 04 (2008) 063.